ELSEVIER

International Journal of Mass Spectrometry 195/196 (2000) 439–457

International Journal of Mass Spectrometry

Absolute alkali metal ion binding affinities of several azines determined by threshold collision-induced dissociation and ab initio theory

R. Amunugama, M.T. Rodgers*

Department of Chemistry, Wayne State University, Detroit, MI 48202, USA

Received 7 June 1999; accepted 13 July 1999

Abstract

Threshold collision-induced dissociation of M^+(azine) with xenon is studied using guided ion beam mass spectrometry. M^+ include the following alkali metal ions: Li^+, Na^+, and K^+. The azines studied include pyridine, pyridazine, pyrimidine, pyrazine, and 1,3,5-triazine. In all cases, the primary product formed corresponds to endothermic loss of the intact azine and the only other product observed is the result of ligand exchange processes to form MXe^+. The cross-section thresholds are interpreted to yield 0 and 298 K bond energies for M^+–azine after accounting for the effects of multiple ion–molecule collisions, internal energy of the reactant ions, and dissociation lifetimes. Ab initio calculations at the MP2(full)/6-311+G(2*d*,2*p*)//MP2(full)/6-31G* level of theory are used to determine the structures of these complexes and provide molecular constants necessary for the thermodynamic analysis of the experimental data. We find that all of the complexes are very nearly planar, the π complexes being significantly less stable. Calculated M^+–azine bond dissociation energies compare favorably to the experimentally determined bond energies for these systems. (Int J Mass Spectrom 195/196 (2000) 439–457)

Keywords: Alkali metal ions; Azines; Binding affinities; Collision-induced dissociation; Guided ion beams

1. Introduction

In recent work, we have developed methods to allow the application of quantitative threshold collision-induced dissociation methods to obtain accurate thermodynamic information on increasingly large systems [1–6]. One of the driving forces behind these developments is our interest in applying such techniques to systems having biological relevance. In addition, we seek to perform accurate thermochemical measurements that provide absolute anchors for the alkali metal cation affinity scales over an ever-broadening range of energies. In the present article, we examine the interactions of the family of six-membered heterocycles containing nitrogen, the azines, with alkali metal ions. Structures of the neutral azine molecules are shown in Fig. 1 along with calculated [7] and measured [8] dipole moments, and estimated polarizabilities [9]. These systems were chosen as models of noncovalent interactions with nucleic acids and a wide variety of nitrogen containing heterocycles of biological importance.

* Corresponding author. E-mail: mrodgers@chem.wayne.edu

In memory of Robert R. Squires and in thanks for his many contributions to gas-phase ion chemistry.

1387-3806/00/$20.00
PII S1387-3806(99)00145-1

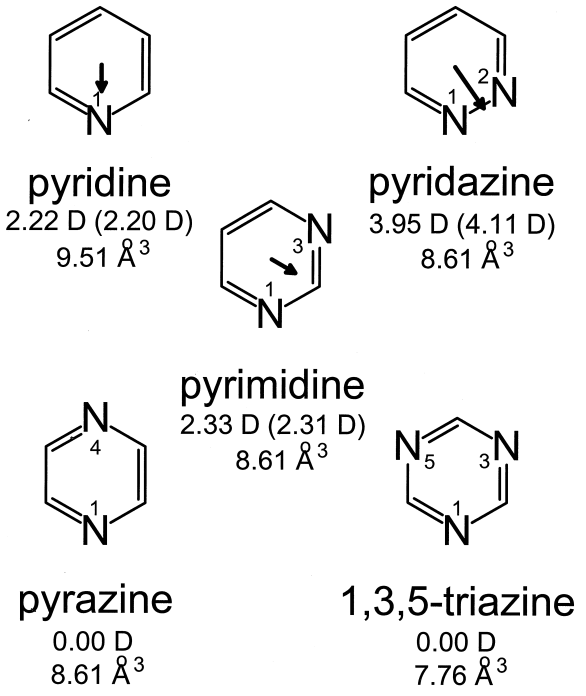

Fig. 1. Structures of the azine molecules. Properly scaled dipole moments in debye are shown as arrows. Values listed are taken from theory [7] and experiment in parentheses [8]. Estimated molecular polarizabilities in Å^3 are also shown [9].

Pyridine is one of the most abundant and best known of the aromatic heterocycles and is produced commercially on a large scale. Compounds containing the pyridine ring are widely distributed in nature. Of these, vitamin B_6 and the nicotinamide adenine dinucleotide phosphates are of the greatest biochemical importance. Pyridine is also the building block of many enzymes, drugs, dyes, and alkaloids [10–13]. Pyridazines are not known to occur in nature and are not easily produced by nitrogen biochemical transformations. However, synthetically produced pyridazines have been useful as growth inhibitors and as medicinals [14,15]. Pyrimidines play a wide variety of roles in biochemical systems. They are the building blocks of the nucleic acids, as well as vitamin B_1, folic acid, barbiturates, antimalarials, oral diuretics, and other pharmaceuticals. They fulfill a series of important functions in biochemical oxidation–reduction processes. They act as dehydrogenases, as one and two-electron transfer reagents, and as activators of molecular O_2. The interaction of pyrimidines with cations is particularly important as σ coordination and π redox reactivity may influence one another [16]. Pyrazines occur commonly in nature with a wide variety of biological activity ranging from flavoring agents, bioluminescent natural products, to pharmaceuticals [17–19]. 1,3,5-Triazines are an unusual class of compound. 1,3,5-Triazine is atypical of its class, being highly reactive and undergoing ring cleavage very easily. 1,3,5-Triazines find widespread use as fiber reactive dyes, optical brighteners, explosives, resins, polymers, fungicides, insecticides, and herbicides. In addition, 1,3,5-Triazines have been used in the treatment of leukemia and as an antitumor drug [20–23].

The azines are members of the class of heteroaromatic compounds referred to as π-deficient *N*-heterocycles [24]. The azines are formed by replacement of one or more of the CH groups in benzene by nitrogen atoms. Because nitrogen is more electronegative than carbon, this leads to a disturbance of the symmetry of the π-electron system, creating a localization of charge on the nitrogen atom(s), decreasing the resonance stabilization and aromatic character of the molecule. The localization of charge on the nitrogen atom(s) make these molecules better proton or cation acceptors and less likely to form cation π complexes. Studies of the interaction of heterocyclic compounds and the azines are of great interest from not only chemical but also pharmacological points of view. The reactivity of heterocyclic bases in the presence of cations may vary in a characteristic way. Thus the site of cation attachment may be closely related to the expression of biological activity and possibly involved directly in receptor–ligand interactions in biological systems.

In the present study, we use guided ion beam mass spectrometry to collisionally excite complexes of Li^+, Na^+, and K^+ bound to five different azines: pyridine (azine), pyridazine (1,2-diazine), pyrimidine (1,3-diazine), pyrazine (1,4-diazine), and 1,3,5-triazine. The kinetic energy dependent cross sections for the collision-induced dissociation (CID) processes are analyzed using methods developed previously [3]. The

analysis explicitly includes the effects of the internal and translational energy distributions of the reactants, multiple collisions, and the lifetime for dissociation. We derive alkali metal cation–azine bond dissociation energies for all the complexes and compare these results to relative values available for Li^+ obtained in equilibrium studies [25] and to *ab initio* calculations performed here and in the literature [7,26,27].

2. Experimental

2.1. General procedures

Cross sections for CID of M^+ (azine), where $M^+ = Li^+$, Na^+, and K^+, and azine = pyridine, pyridazine, pyrimidine, pyrazine, and 1,3,5-triazine, are measured using a guided ion beam mass spectrometer that has been described in detail previously [28,29]. The metal ligand complexes are generated as described in the following. The ions are extracted from the source, accelerated, and focused into a magnetic sector momentum analyzer for mass analysis. Mass-selected ions are decelerated to a desired kinetic energy and focused into an octopole ion guide, which traps the ions in the radial direction [30]. The octopole passes through a static gas cell containing xenon, used as the collision gas, for reasons described elsewhere [31–33]. Low gas pressures in the cell (typically 0.04–0.20 m Torr) are used to ensure that multiple ion–molecule collisions are improbable. Product and unreacted beam ions drift to the end of the octopole where they are focused into a quadrupole mass filter for mass analysis and subsequently detected with a secondary electron scintillation detector and standard pulse counting techniques.

Ion intensities are converted to absolute cross sections as described previously [28]. Absolute uncertainties in cross section magnitudes are estimated to be ±20%, which are largely the result of errors in the pressure measurement and the length of the interaction region. Relative uncertainties are approximately ±5%. Because the radio frequency used for the octopole does not trap light masses with high efficiency, the cross sections for Li^+ products were more scattered and showed more variations in magnitude than is typical for this apparatus. Therefore, absolute magnitudes of the cross sections for production of Li^+ are probably ±50%.

Ion kinetic energies in the laboratory frame, E_{lab}, are converted to energies in the center of mass frame, E_{CM}, using the formula $E_{CM} = E_{lab}m/(m + M)$, where M and m are the masses of the ionic and neutral reactants, respectively. All energies reported below are in the CM frame unless otherwise noted. The absolute zero and distribution of the ion kinetic energies are determined using the octopole ion guide as a retarding potential analyzer as previously described [28]. The distribution of ion kinetic energies is nearly Gaussian with a full width at half maximum typically between 0.2 and 0.4 eV (lab) for these experiments. The uncertainty in the absolute energy scale is ±0.05 eV (lab).

Even when the pressure of the reactant neutral is low, we have previously demonstrated that the effects of multiple collisions can significantly influence the shape of CID cross sections [34]. Because the presence and magnitude of these pressure effects is difficult to predict, we have performed pressure dependent studies of all cross sections examined here. In the present systems, we observe small cross sections at low energies that have an obvious dependence upon pressure. We attribute this to multiple energizing collisions that lead to an enhanced probability of dissociation below threshold as a result of the longer residence time of these slower moving ions. Data free from pressure effects are obtained by extrapolating to zero reactant pressure, as described previously [34]. Thus, results reported in the following are due to single bimolecular encounters.

2.2. Ion source

The M^+(azine) complexes are formed in a 1-m-long flow tube [29,35] operating at a pressure of 0.5–0.7 Torr with a helium flow rate of 4000–7000 sccm. Metal ions are generated in a continuous dc discharge by argon ion sputtering of a cathode, made from tantalum or iron, with a cavity containing the alkali metal. Typical operating conditions of the

discharge are 2–3 kV and 20–30 mA in a flow of roughly 10% argon in helium. The M^+(azine) complexes are formed by associative reactions of the alkali metal ion with the neutral azine, which is introduced into the flow 50 cm downstream from the dc discharge. In all cases except for pyridazine, the vapor pressure of each of the azines was sufficient to produce enough vaporized ligand to carry out these experiments. Pyridazine required gentle heating and a flow of helium over the sample to vaporize. The flow conditions used in this ion source provide in excess of 10^4 collisions between an ion and the buffer gas, which should thermalize the ions both vibrationally and rotationally. In our analysis of the data, we assume that the ions produced in this source are in their ground electronic states and that the internal energy of the M^+(azine) complexes is well described by a Maxwell-Boltzmann distribution of ro-vibrational states at 300 K. Previous work has shown that these assumptions are generally valid [31,34–38].

2.3. Thermochemical analysis

The threshold regions of the reaction cross sections are modeled by using

$$\sigma(E) = \sigma_0 \sum_i g_i(E + E_i - E_0)^n/E \quad (1)$$

where σ_0 is an energy independent scaling factor, E is the relative translational energy of the reactants, E_0 is the threshold for reaction of the ground electronic and ro-vibrational state, and n is an adjustable parameter. The summation is over the ro-vibrational states of the reactant ions, i, where E_i is the excitation energy of each state and g_i, is the population of those states ($\sum g_i = 1$). The populations of excited ro-vibrational levels are not negligible even at 300 K as a result of the many low-frequency modes present in these ions. The relative reactivity of all ro-vibrational states, as reflected by σ_0 and n, is assumed to be equivalent.

To obtain model structures, vibrational frequencies, and energetics for the neutral and metalated azines, *ab initio* calculations were performed using GAUSSIAN 98 [39]. Geometry optimizations were performed at the MP2(full)/6-31G* level. This level of theory was recently determined by Hoyau et al. [40] and us [6] to be adequate for a good description of sodium cation complexes. This conclusion is reinvestigated here and tested for lithium, sodium and potassium cation complexes. Vibrational analyses of the geometry-optimized structures were performed to determine the vibrational frequencies and rotational constants of the molecules. When used to model the data or to calculate thermal energy corrections, the MP2(full)/6-31G* vibrational frequencies are scaled by a factor of 0.9646 [41,42]. The scaled vibrational frequencies thus obtained for the 15 systems studied are listed in Table 1, whereas Table 2 lists the rotational constants. Single point energy calculations were performed at the MP2(full)/6-311+G($2d$,$2p$) level using the MP2(full)/6-31G* geometries. To obtain accurate bond dissociation energies, basis set superposition errors (BSSE) were subtracted from the computed dissociation energies in the full counterpoise approximation [43,44], as in several other recent papers on Na^+ complexes [45,46]. The BSSE corrections ranged from 3.2 kJ/mol for K^+(1,3,5-triazine) to 8.3 kJ/mol for the Li^+(pyridazine) complex.

The Beyer-Swinehart algorithm [47] is used to evaluate the density of the ro-vibrational states and the relative populations g_i are calculated by an appropriate Maxwell-Boltzmann distribution at the 300 K temperature appropriate for the reactants. The average vibrational energy at 298 K of the alkali metal ion bound azines is also given in Table 1. We have estimated the sensitivity of our analysis to the deviations from the true frequencies by scaling the calculated frequencies to encompass the range of average valence coordinate scale factors needed to bring calculated frequencies into agreement with experimentally determined frequencies found by Pople *et al*. [48]. Thus, the originally calculated vibrational frequencies were increased and decreased by 10%. The corresponding change in the average vibrational energy is taken to be an estimate of one standard deviation of the uncertainty in vibrational energy (Table 1) and is included in the uncertainties listed with the E_0 values.

We also consider the possibility that collisionally activated complex ions do not dissociate on the time

Table 1
Vibrational frequencies and average vibrational energies at 298 K[a]

Species	E_{vib} (eV)[b]	Frequencies (cm^{-1})[c]
Pyridine	0.05 (0.01)	366, 392, 591, 646, 661, 713, 861, 899, 906, 926, 981, 1022, 1063, 1075, 1165, 1226, 1356, 1365, 1449, 1484, 1594, 1603, 3105, 3106, 3120, 3135, 3142
Li^+(pyridine)	0.09 (0.01)	115, 148, 370, 395, 435, 641, 643, 658, 722, 865, 893, 918, 940, 1008, 1028, 1074, 1078, 1179, 1231, 1360, 1377, 1466, 1495, 1590, 1628, 3118, 3119, 3142, 3155, 3159
Na^+(pyridine)	0.10 (0.01)	73, 86, 222, 370, 393, 613, 642, 658, 718, 866, 890, 915, 936, 1000, 1024, 1073, 1076, 1177, 1231, 1359, 1375, 1462, 1494, 1591, 1622, 3112, 3113, 3140, 3152, 3157
K^+(pyridine)	0.11 (0.01)	57, 59, 151, 370, 393, 607, 643, 661, 718, 868, 891, 915, 931, 995, 1025, 1073(2), 1175, 1231, 1358, 1374, 1459, 1493, 1591, 1619, 3103, 3104, 3137, 3149, 3154
Pyridazine	0.04 (0.04)	349, 358, 607, 656, 681, 737, 902, 914, 917, 966, 1032, 1067, 1070, 1158, 1270, 1280, 1404, 1451, 1574, 1578, 3121, 3127, 3136, 3146
Li^+(pyridazine)	0.08 (0.01)	159, 235, 357, 382, 469, 618, 675, 680, 758, 917, 939, 940, 969, 1046, 1059, 1092, 1175, 1284, 1329, 1419, 1463, 1576, 1596, 3147, 3154, 3160, 3164
Na^+(pyridazine)	0.09 (0.01)	102, 129, 247, 353, 375, 614, 660, 679, 754, 915, 934, 935, 965, 1046, 1063, 1084, 1171, 1284, 1313, 1416, 1462, 1578, 1592, 3144, 3148, 3155, 3162
K^+(pyridazine)	0.10 (0.01)	85, 114, 180, 353, 376, 614, 659, 685, 753, 916, 934, 936, 966, 1046, 1066, 1080, 1169, 1285, 1307, 1414, 1461, 1578, 1589, 3140, 3144, 3152, 3160
Pyrimidine	0.04 (0.01)	339, 394, 608, 670, 712, 787, 915, 947, 959, 981, 1054, 1075, 1136, 1221, 1298, 1372, 1410, 1467, 1580, 1587, 3111, 3114, 3128, 3150
Li^+(pyrimidine)	0.08 (0.01)	120, 155, 336, 401, 427, 629, 683, 705, 793, 923, 937, 972, 1004, 1049, 1086, 1136, 1227, 1308, 1381, 1420, 1476, 1571, 1612, 3121, 3127, 3140, 3166
Na^+(pyrimidine)	0.10 (0.01)	77, 90, 212, 337, 399, 619, 672, 708, 789, 921, 937, 968, 994, 1050, 1084, 1136, 1227, 1307, 1381, 1417, 1475, 1573, 1607, 3116, 3123, 3138, 3164
K^+(pyrimidine)	0.10 (0.01)	60, 63, 143, 338, 398, 616, 671, 711, 790, 921, 941, 965, 990, 1052, 1082, 1136, 1226, 1307, 1381, 1414, 1475, 1574, 1603, 3109, 3116, 3136, 3162
Pyrazine	0.04 (0.01)	333, 412, 585, 694, 727, 777, 915, 922, 933, 1005, 1006, 1075, 1136, 1237, 1319, 1348, 1421, 1479, 1536, 1585, 3112(2), 3126, 3130
Li^+(pyrazine)	0.09 (0.01)	118, 153, 331, 419, 423, 632, 688, 718, 776, 887, 923, 949, 1001, 1037, 1087, 1124, 1243, 1334, 1355, 1429, 1482, 1530, 1601, 3128(2), 3145, 3148
Na^+(pyrazine)	0.10 (0.01)	76, 90, 210, 332, 418, 604, 689, 718, 775, 892, 921, 946, 1003, 1024, 1085, 1127, 1243, 1330, 1354, 1427, 1482, 1531, 1597, 3123, 3124, 3142, 3145
K^+(pyrazine)	0.10 (0.01)	59, 64, 142, 332, 417, 598, 691, 722, 776, 898, 921, 944, 1005, 1018, 1083, 1128, 1242, 1326, 1353, 1426, 1483, 1532, 1595, 3116, 3117, 3138, 3141
1,3,5-Triazine	0.04 (0.01)	347(2), 665(2), 744, 893, 981, 991(2), 1113, 1171(2), 1214, 1382, 1420(2), 1567(2), 3129(2), 3133
Li^+(1,3,5-triazine)	0.08 (0.01)	122, 162, 347, 349, 418, 653, 697, 730, 898, 974, 1000, 1007, 1099, 1162, 1166, 1232, 1389, 1420, 1438, 1546, 1599, 3129, 3130, 3159
Na^+(1,3,5-triazine)	0.09 (0.01)	80, 93, 202, 344, 349, 656, 681, 734, 893, 975, 991, 1003, 1102, 1165, 1167, 1227, 1389, 1418, 1436, 1549, 1592, 3126, 3127, 3157
K^+(1,3,5-triazine)	0.10 (0.01)	63, 66, 133, 345, 349, 659, 676, 738, 894, 979, 988, 1001, 1106, 1167, 1224, 1388, 1417, 1435, 1552, 1588, 3121, 3123, 3155

[a] Vibrational frequencies (scaled by 0.9646) are obtained from a vibrational analysis of the geometry optimized structures for these species obtained from *ab initio* calculations performed at the MP2(full)/6-31G* level.
[b] Uncertainties listed in parentheses are determined as described in the text.
[c] Degeneracies in parentheses.

scale of our experiment (about 10^{-4} s) by including statistical theories for unimolecular dissociation into Eq. (1) as described in detail elsewhere [3,36]. This requires sets of ro-vibrational frequencies appropriate for the energized molecules and the transition states (TSs) leading to dissociation. The former are given in Tables 1 and 2 whereas we assume that the TSs are loose and product like because the interaction between the alkali metal ion and the ligand is largely electrostatic. In this case, the TS vibrations used are the frequencies corresponding to the products, which are also found in Table 1. The transitional frequen-

Table 2
Rotational constants of M^+(azine) in cm^{-1}

	Energized molecule		Transition state		
Reactant	1D[a]	2D[b]	1D[c]	2D[c]	2D[b,d]
Li^+(pyridine)	0.20	0.086	0.099	0.20	0.033
Na^+(pyridine)	0.20	0.045	0.099	0.20	0.0065
K^+(pyridine)	0.20	0.029	0.099	0.20	0.0038
Li^+(pyridazine)	0.20	0.094	0.10	0.20	0.041
Na^+(pyridazine)	0.20	0.051	0.10	0.20	0.0076
K^+(pyridazine)	0.21	0.033	0.10	0.20	0.0048
Li^+(pyrimidine)	0.20	0.088	0.10	0.21	0.034
Na^+(pyrimidine)	0.21	0.046	0.10	0.21	0.0065
K^+(pyrimidine)	0.21	0.029	0.10	0.21	0.0037
Li^+(pyrazine)	0.21	0.086	0.10	0.20	0.033
Na^+(pyrazine)	0.21	0.045	0.10	0.20	0.0068
K^+(pyrazine)	0.21	0.029	0.10	0.20	0.0037
Li^+(1,3,5-triazine)	0.21	0.090	0.11	0.21	0.034
Na^+(1,3,5-triazine)	0.21	0.046	0.11	0.21	0.0068
K^+(1,3,5-triazine)	0.21	0.029	0.11	0.21	0.0038

[a] Active external.
[b] Inactive external.
[c] Rotational constants of the transition state treated as free internal rotors.
[d] Treated variationally. Value cited is obtained at the threshold energy for dissociation.

cies, those that become rotations of the completely dissociated products, are treated as rotors, a treatment that corresponds to a phase space limit (PSL) and is described in detail elsewhere [3]. For the M^+(azine) complexes, the two transitional mode rotors have rotational constants equal to those of the neutral azine product with axes perpendicular to the reaction coordinate. These are listed in Table 2. The external rotations of the energized molecule and TS are also included in the modeling of the CID data. The external rotational constants of the TS are determined by assuming that the TS state occurs at the centrifugal barrier for interaction of M^+ with the neutral azine, calculated variationally as outlined elsewhere [3]. The two-dimensional (2-D) external rotations are treated adiabatically but with centrifugal effects included, consistent with the discussion of Waage and Rabinovitch [49]. In the present work, the adiabatic 2-D rotational energy is treated using a statistical distribution with explicit summation over the possible values of the rotational quantum number, as described in detail elsewhere [3].

The model represented by Eq. (1) is expected to be appropriate for translationally driven reactions [50] and has been found to reproduce reaction cross sections well in a number of previous studies of both atom–diatom and polyatomic reactions [51,52], including CID processes [1,2,31,34–36,53–55]. The model is convoluted with the kinetic energy distributions of both reactants, and a nonlinear least-squares analysis of the data is performed to give optimized values for the parameters σ_0, E_0, and n. The error associated with the measurement of E_0 is estimated from the range of threshold values determined for different data sets, variations associated with uncertainties in the vibrational frequencies, and the error in the absolute energy scale, 0.05 eV (lab). For analyses that include the Rice-Ramsperger-Kassel-Marcus (RRKM) lifetime effect, the uncertainties in the reported E_0 values also include the effects of increasing and decreasing the time assumed available for dissociation (10^{-4} s) by a factor of 2.

Equation (1) explicitly includes the internal energy of the ion, E_i. All energy available is treated statistically, which should be a reasonable assumption because the internal (rotational and vibrational) energy of the reactants is redistributed throughout the ion upon impact with the collision gas. The threshold for dissociation is by definition the minimum energy required leading to dissociation and thus corresponds to formation of products with no internal excitation. The assumption that products formed at threshold have an internal temperature of 0 K has been tested for several systems [1,2,31,34–36]. It has been shown that treating all energy of the ion (vibrational, rotational, and translational) as capable of coupling into the dissociation coordinate leads to reasonable thermochemistry. The threshold energies for dissociation reactions determined by analysis with Eq. (1) are converted to 0 K bond energies by assuming that E_0 represents the energy difference between reactants and products at 0 K [56]. This requires that there are no activation barriers in excess of the endothermicity

of dissociation. This is generally true for ion–molecule reactions [51] and should be valid for the simple heterolytic bond fission reactions examined here [57].

3. Results

3.1. Cross sections for collision-induced dissociation

Experimental cross sections were obtained for the interaction of Xe with 15 M^+(azine) complexes, where $M^+ = Li^+$, Na^+, and K^+ azine = pyridine, pyridazine, pyrimidine, pyrazine, and 1,3,5-triazine. Fig. 2 shows representative data for the M^+(pyrimidine) complexes with all three metals. As discussed previously, the nonzero cross sections observed in these data at the lowest energies are a consequence of multiple collisions and disappear when the data are extrapolated to zero pressure of the Xe reactant as shown in Fig. 2. The other azine complexes show similar relative behavior. The most favorable process for all complexes is the loss of the intact azine molecule in the (CID) reaction

$$M^+(\text{azine}) + Xe \rightarrow M^+ + \text{azine} + Xe \qquad (2)$$

The magnitudes of the cross sections generally increase in size from $M^+ = Li^+$ to Na^+ to K^+. This is largely because the thresholds decrease in this same order. The only other products that are observed in these reactions are the result of ligand exchange processes to form MXe^+. The cross sections for these products are approximately one to two orders of magnitude smaller than those for the primary M^+ product, and the thresholds are slightly lower (by the M^+–Xe binding energy). As little systematic information can be gleaned from these products, they will not be discussed further. However, it is conceivable that this ligand exchange process might cause a competitive shift in the observed thresholds. Within the quoted experimental errors, we do not believe such competition is likely to affect our threshold measurements in any of these systems for several reasons that have been detailed elsewhere [58].

3.2. Threshold analysis

The model of Eq. (1) was used to analyze the thresholds for reactions (2) in 15 M^+(azine) systems. The results of these analyses are provided in Table 3 and representative results are shown in Fig. 3 for the M^+(pyrimidine) complexes with all three metals. In all cases, the experimental cross sections for reaction (2) are accurately reproduced using a loose PSL TS model [3]. Previous work has shown that this model provides the most accurate assessment of the kinetic shifts for CID processes for electrostatic ion–molecule complexes [1–4,53,54]. Good reproduction of the data is obtained over energy ranges exceeding 3 eV and cross section magnitudes of at least a factor of 100. Table 3 also includes values of E_0 obtained without including the RRKM lifetime analysis. Comparison of these values with the E_0(PSL) values shows that the kinetic shifts are negligibly small in all of the K^+ complexes as well as the Li^+ and Na^+ complexes with pyrazine and triazine. In the more strongly bound systems, the kinetic shift for the Li^+ complexes varied between 0.01 and 0.15 eV, whereas it only varied between 0.01 and 0.02 eV for the Na^+ complexes. Although the total number of vibrations changes for the azines (27 for pyridine, 24 for pyridazine, pyrimidine, and pyrazine, and 21 for 1,3,5-triazine), the number of heavy atoms in these molecules (and hence the number of lower frequency vibrations) remains the same. This explains the similarity in the kinetic shifts as the azine is varied. The rigidity of the aromatic azines is a contributing factor to the small magnitudes of the kinetic shifts.

The entropy of activation, $\Delta S^\dagger$, is a measure of the looseness of the TS and also a reflection of the complexity of the system. It is largely determined by the molecular parameters used to model the energized molecule and the TS, but also depends upon the threshold energy. Listed in Table 3, $\Delta S^\dagger$(PSL) values at 1000 K can be seen to decrease from the Li to the Na to the K systems. These entropies of activation can be favorably compared to $\Delta S^\dagger_{1000}$ values in the range of 29–46 J/K mol collected by Lifshitz for several simple bond cleavage dissociations of ions [59].

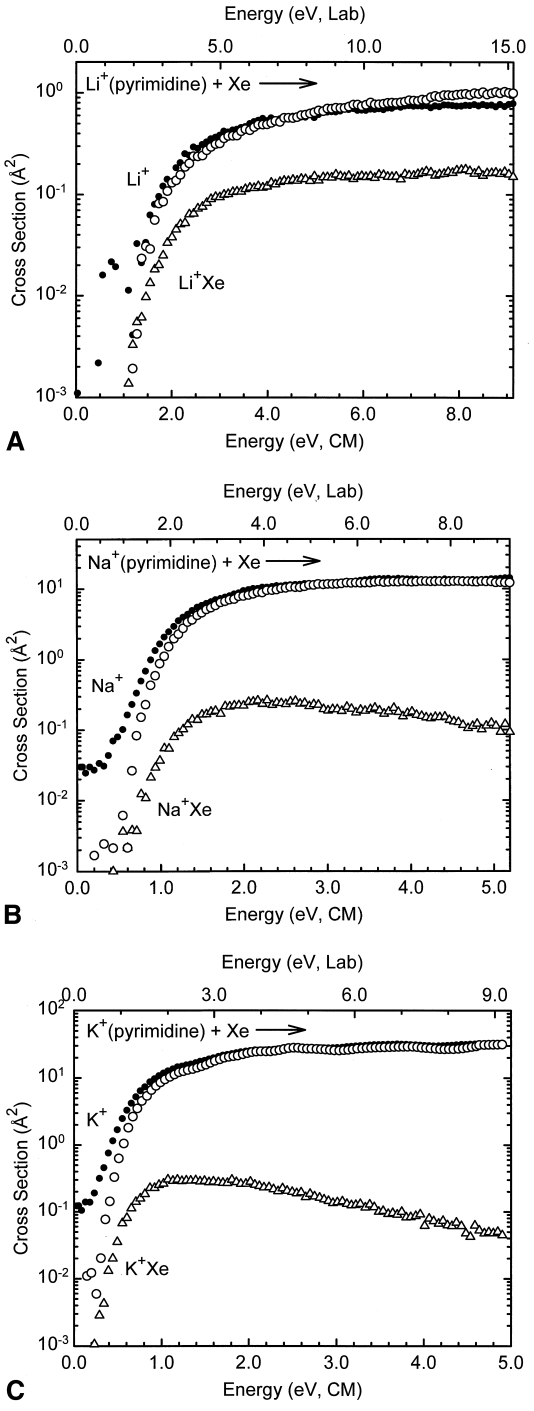

Fig. 2. Cross sections for collision-induced dissociation of M^+(pyrimidine) complexes where $M^+ = Li^+$, Na^+, and K^+ (parts a, b, and c, respectively) with Xe as a function of kinetic energy in the center-of-mass frame (lower *x* axis) and the laboratory frame (upper *x* axis). Data are shown for a xenon pressure of ~20 mTorr (closed circle) and extrapolated to zero (open circle). Cross sections for the ligand exchange process to form M^+Xe are also shown (open triangle).

3.3. Theoretical results

Theoretical structures for the neutral azines (pyridine, pyridazine, pyrimidine, pyrazine, and 1,3,5-triazine), and for the complexes of these species with H^+, Li^+, Na^+, and K^+ were calculated as described previously. Table 4 gives details of the final geometries for each of these species. Results for the most stable conformations of the lithium metal ion–azine complexes are shown in Fig. 4 [60].

Not surprisingly, the calculations find that the proton or metal ion prefers to be bound to the nitrogen atom rather than the π cloud of the aromatic ring for all of the azines. In some cases, stable conformations corresponding to the metal ion binding to the π cloud of the azine molecule were found, but these species were considerably less stable. In other cases, the starting π-complex geometries always converged to the more energetically favorable planar geometry. For the pyridine, pyrimidine, pyrazine, and 1,3,5-triazine complexes, the proton or metal binds to a single nitrogen atom. The binding observed in the pyridazine system differs somewhat. In the protonated system, the proton binds to a single nitrogen atom, whereas the metal ion bridges the two adjacent nitrogen atoms in the metalated systems. In general, the distortion of the azine molecule that occurs upon complexation to a proton or alkali metal cation is minor. The change in geometry is the largest for the protonated systems and decreases with increasing size of the cation. Bond lengths and angles change in the most extreme cases by less than 0.02 Å and 7.5°, respectively.

The 0 K calculated proton and metal binding energies, performed at the MP2(full)/6-311+G(2*d*,2*p*)//MP2(full)/6-31G* level including full MP2 correlation, zero point energy corrections and basis set superposition error corrections [61–63],

Table 3
Threshold dissociation energies at 0 K and entropies of activation at 1000 K of M^+(azine)[a]

Reactant complex	σ_0[b]	n[b]	E_0[c] (eV)	E_0(PSL) (eV)	$\Delta S^{\ddagger}$(PSL) (J mol^{-1} K^{-1})
Li^+(pyridine)	0.5 (0.2)	1.4 (0.2)	1.95 (0.19)	1.88 (0.15)	32 (2)
Na^+(pyridine)	13.7 (0.2)	1.2 (0.1)	1.32 (0.03)	1.31 (0.03)	26 (2)
K^+(pyridine)	34.8 (0.8)	1.3 (0.1)	0.94 (0.04)	0.94 (0.04)	18 (2)
Li^+(pyridazine)	0.5 (0.1)	1.3 (0.1)	2.59 (0.13)	2.43 (0.11)	39 (2)
Na^+(pyridazine)	11.7 (0.2)	1.3 (0.1)	1.67 (0.03)	1.65 (0.03)	33 (2)
K^+(pyridazine)	29.6 (0.4)	1.1 (0.1)	1.38 (0.03)	1.38 (0.03)	28 (2)
Li^+(pyrimidine)	0.7 (0.1)	1.2 (0.1)	1.61 (0.12)	1.60 (0.11)	32 (2)
Na^+(pyrimidine)	14.3 (0.3)	1.4 (0.1)	1.07 (0.04)	1.06 (0.04)	25 (2)
K^+(pyrimidine)	28.3 (0.7)	1.4 (0.1)	0.72 (0.05)	0.72 (0.05)	18 (2)
Li^+(pyrazine)	0.4 (0.1)	1.5 (0.1)	1.55 (0.15)	1.55 (0.14)	31 (2)
Na^+(pyrazine)	16.4 (0.4)	1.1 (0.1)	1.11 (0.04)	1.11 (0.04)	25 (2)
K^+(pyrazine)	30.0 (0.9)	1.2 (0.1)	0.70 (0.04)	0.70 (0.04)	18 (2)
Li^+(1,3,5-triazine)	0.6 (0.1)	1.4 (0.1)	1.32 (0.13)	1.32 (0.13)	31 (2)
Na^+(1,3,5-triazine)	16.3 (0.1)	1.2 (0.1)	0.92 (0.03)	0.92 (0.03)	24 (2)
K^+(1,3,5-triazine)	28.1 (0.1)	1.3 (0.1)	0.57 (0.03)	0.57 (0.03)	17 (2)

[a] Uncertainties are listed in parentheses.
[b] Average values for loose PSL transition state.
[c] No RRKM analysis.

are listed in Table 5. In all of the azine systems, the binding strength varies with the metal ion such that Li^+ binds ~50% more strongly than Na^+, which in turn binds ~40% more strongly than K^+. As these complexes are largely electrostatic in nature, this is easily understood based upon the size or equivalently the charge density on the metal. The smaller the ion, the greater the charge density of the metal and therefore the greater the strength of the ion–dipole or ion–induced dipole interaction in these systems. The binding energy increases with decreasing charge on the metal. For a given azine, the charge retained on the metal follows the order Li^+ ($\sim 0.75e$) < Na^+ ($\sim 0.92e$) < K^+ ($\sim 0.98e$). The shorter bond distance and greater charge density in the smaller cations allows the metal ion to more effectively withdraw electron density from the neutral ligand thus reducing the charge retained on the metal and increasing the covalency of the metal-ligand interaction. These results are discussed in further detail in the following.

3.3.1. Pyridine

Pyridine is the simplest of the azine systems studied here. Pyridine possesses only a single strongly basic site (at N1). Indeed, this site is calculated and measured [64,65] to be the most basic of all the azines consider here, having a protonation energy at 0 K of 908.9 kJ/mol (calculated) and 924.0 ± 16.0 kJ/mol (measured at 298 K, adjusted to 0 K). Consistent with this, we find that the calculated metal ion binding energies for this molecule are the strongest of the monoligated species examined here, and as expected the metal binds to the same site (N1).

A stable cation π complex of Li^+ to pyrimidine was found. However, this complex was found to be 67.0 kJ/mol less stable than the planar geometry. Attempts to calculate stable cation π complexes of pyridine to Na^+ or K^+ always converged to the energetically more favorable planar geometry. The large energy difference in the binding of Li^+ in the planar versus π complexes and the inability to find stable π complexes to Na^+ and K^+ suggests that there is only a single possible geometry for the M^+ (pyridine) complexes. Further, because of the strong ion–dipole and ion–induced dipole interactions, the potential energy surface for M^+ + pyridine should be attractive with no barriers in excess of the bond energy.

3.3.2. Pyridazine

Proton and metal ion binding to the diazines and triazine is somewhat more complicated in that each

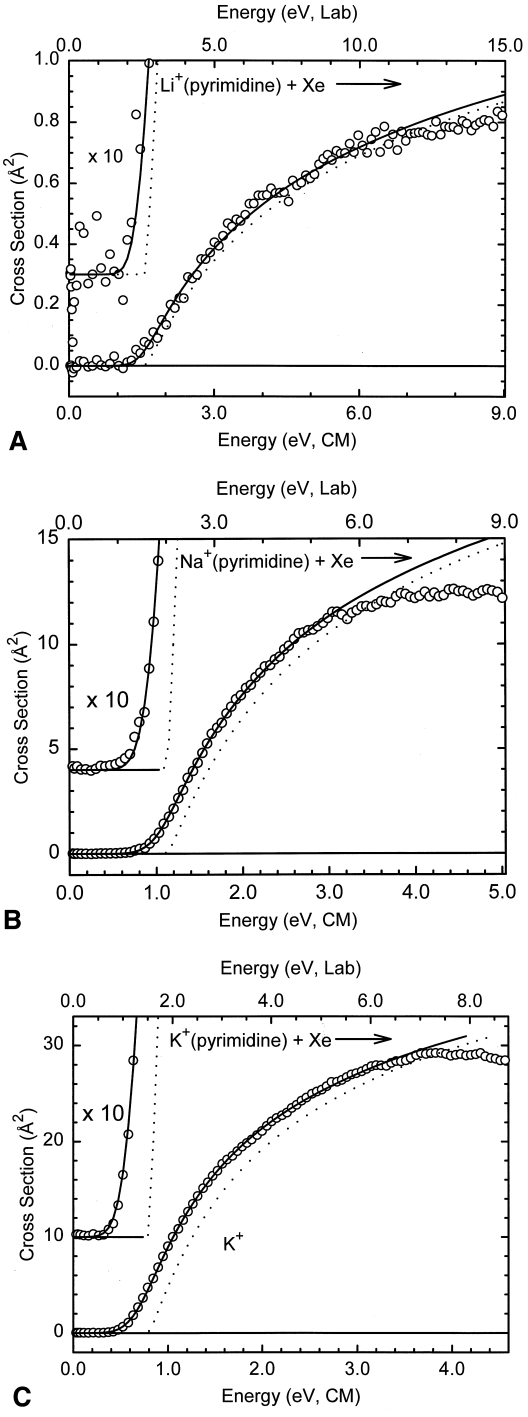

Fig. 3. Zero pressure extrapolated cross sections for collision-induced dissociation of M^+(pyrimidine) complexes where M^+ = Li^+, Na^+, and K^+ (parts a, b, and c, respectively) with Xe in the threshold region as a function of kinetic energy in the center-of-mass frame (lower *x* axis) and the laboratory frame (upper *x* axis). Solid lines show the best fits to the data using the model of Eq. (1) convoluted over the neutral and ion kinetic and internal energy distributions. Dashed lines show the model cross sections in the absence of experimental kinetic energy broadening for reactants with an internal energy of 0 K.

possesses more than one basic site. Protonation of pyridazine (1,2-diazine) at either nitrogen atom produces the same protonated complex with a calculated protonation enthalpy at 0 K of 894.2 kJ/mol. The previously measured proton affinity of pyridazine, adjusted to 0 K, is 901.1 ± 16.0 kJ/mol [64,65]. These values are somewhat lower than that determined for pyridine suggesting that the presence of the second nitrogen atom (electron withdrawing group) results in a decrease in the electron density on the binding nitrogen, weakening its attraction for the proton. However, when compared to the other diazines (pyrimidine and pyrazine, discussed below), the proton and metal cation binding affinities are higher. Pyridazine is the only system where these basic sites are adjacent. Enhanced proton and metal ion binding in the pyridazine system is easily rationalized because geometries possessing in-plane lone pairs of electrons on adjacent nitrogen atoms are less stable in the neutral systems, whereas this creates a more favorable geometry for proton and metal ion binding. This is particularly important in the metal ion systems as they are much larger than a proton and capable of chelation (multiple donor) interactions resulting in significant increases in the binding energies. Indeed, the alkali metal ion binding affinities of pyridazine are significantly greater than for any of the other azines examined here. Attempts to calculate stable cation π complexes to pyridazine also always converged to the energetically more favorable planar geometry. Overall, we conclude that there is only a single stable geometry for the M^+(pyridazine) complexes.

3.3.3. Pyrimidine

Pyrimidine (1,3-diazine) also possesses two basic nitrogen atoms. Protonation of pyrimidine at either

Table 4
MP2(full)/6-31G* geometry optimized structures of the neutral, protonated, and alkali metalated azines[a]

	Bond length (Å)											
Species	1–2	2–3	3–4	4–5	5–6	6–1	1–*X*	2–*X*	3–*X*	4–*X*	5–*X*	6–*X*
Pyridine	1.344	1.394	1.393	1.393	1.394	1.344	. . .	1.088	1.086	1.087	1.086	1.088
H^+(pyridine)	1.350	1.386	1.396	1.396	1.386	1.350	**1.022**	1.084	1.085	1.086	1.085	1.084
Li^+(pyridine)	1.354	1.389	1.393	1.393	1.389	1.354	**1.967**	1.087	1.065	1.086	1.085	1.087
Na^+(pyridine)	1.352	1.390	1.393	1.393	1.390	1.352	**2.326**	1.088	1.085	1.086	1.085	1.088
K^+(pyridine)	1.350	1.391	1.393	1.393	1.391	1.350	**2.732**	1.088	1.085	1.086	1.085	1.088
Pyridazine	1.347	1.343	1.396	1.385	1.396	1.343	. . .	. . .	1.087	1.087	1.087	1.087
H^+(pyridazine)	1.329	1.340	1.401	1.389	1.393	1.340	**1.025**	. . .	1.085	1.086	1.085	1.085
Li^+(pyridazine)	1.352	1.339	1.397	1.388	1.397	1.339	**1.984**	**1.984**	1.085	1.085	1.085	1.085
Na^+(pyridazine)	1.354	1.340	1.397	1.386	1.397	1.340	**2.348**	**2.348**	1.086	1.086	1.086	1.086
K^+(pyridazine)	1.353	1.341	1.397	1.386	1.397	1.341	**2.712**	**2.712**	1.086	1.085	1.085	1.086
Pyrimidine	1.341	1.341	1.342	1.391	1.391	1.342	. . .	1.087	. . .	1.088	1.085	1.088
H^+(pyrimidine)	1.353	1.321	1.344	1.397	1.383	1.350	**1.023**	1.086	. . .	1.087	1.084	1.085
Li^+(pyrimidine)	1.352	1.329	1.342	1.394	1.387	1.353	**1.986**	1.088	. . .	1.087	1.084	1.087
Na^+(pyrimidine)	1.350	1.331	1.342	1.393	1.388	1.351	**2.351**	1.088	. . .	1.087	1.085	1.087
K^+(pyrimidine)	1.348	1.333	1.342	1.393	1.388	1.350	**2.764**	1.089	. . .	1.087	1.085	1.088
Pyrazine	1.343	1.394	1.343	1.343	1.394	1.343	. . .	1.088	1.088	. . .	1.088	1.088
H^+(pyrazine)	1.348	1.394	1.341	1.341	1.394	1.348	**1.024**	1.084	1.086	. . .	1.086	1.084
Li^+(pyrazine)	1.352	1.393	1.341	1.341	1.393	1.352	**1.988**	1.087	1.087	. . .	1.087	1.087
Na^+(pyrazine)	1.351	1.393	1.341	1.341	1.393	1.351	**2.353**	1.087	1.087	. . .	1.087	1.087
K^+(pyrazine)	1.349	1.394	1.342	1.342	1.394	1.349	**2.766**	1.087	1.087	. . .	1.087	1.087
1,3,5-Triazine	1.339	1.339	1.339	1.339	1.339	1.339	. . .	1.088	. . .	1.088	. . .	1.088
H^+(1,3,5-triazine)	1.353	1.319	1.344	1.344	1.319	1.353	**1.025**	1.087	. . .	1.087	. . .	1.087
Li^+(1,3,5-triazine)	1.352	1.328	1.341	1.341	1.328	1.352	**2.004**	1.088	. . .	1.086	. . .	1.088
Na^+(1,3,5-triazine)	1.349	1.330	1.340	1.340	1.330	1.349	**2.375**	1.088	. . .	1.086	. . .	1.088
K^+(1,3,5-triazine)	1.347	1.332	1.340	1.340	1.332	1.347	**2.802**	1.088	. . .	1.086	. . .	1.088
	Bond angle (deg)											
Species	123	234	345	451	561	612	*X*12	*X*23	*X*34	*X*45	*X*56	*X*61
Pyridine	123.8	118.7	118.4	118.7	123.8	116.8	. . .	120.5	121.2	120.8	120.2	115.7
H^+(pyridine)	118.8	119.4	119.8	119.4	118.8	123.8	**118.1**	124.2	121.4	120.1	119.2	117.0
Li^+(pyridine)	122.7	119.0	118.8	119.0	122.7	117.9	**120.9**	120.6	121.3	120.6	119.7	116.7
Na^+(pyridine)	123.0	118.9	118.6	118.9	123.0	117.4	**121.2**	120.3	121.3	120.7	119.8	116.6
K^+(pyridine)	123.5	118.8	118.5	118.8	123.5	116.9	**121.5**	120.1	121.3	120.7	119.9	116.5
Pyridazine	119.0	124.1	116.9	116.9	124.1	119.0	. . .	. . .	121.4	122.2	120.9	114.5
H^+(pyridazine)	114.8	123.6	118.5	117.8	118.1	127.3	**112.6**	. . .	122.5	121.3	120.0	116.9
Li^+(pyridazine)	120.2	121.9	118.0	118.0	121.9	120.2	**70.1**	**169.8**	122.8	121.7	120.3	115.4
Na^+(pyridazine)	119.7	122.6	117.7	117.7	122.6	119.7	**73.2**	**167.0**	122.2	121.9	120.4	115.1
K^+(pyridazine)	119.5	123.1	117.4	117.4	123.1	119.5	**75.6**	**165.0**	121.9	122.0	120.6	115.0
Pyrimidine	127.3	115.6	122.3	116.9	122.3	115.6	. . .	116.3	. . .	121.4	121.6	116.3
H^+(pyrimidine)	122.1	117.6	122.8	117.8	117.6	122.1	**118.6**	120.4	. . .	121.2	120.5	117.5
Li^+(pyrimidine)	126.2	116.6	122.1	117.3	121.3	116.5	**119.5**	116.6	. . .	121.6	121.0	117.3
Na^+(pyrimidine)	126.6	116.4	122.0	117.2	121.7	116.1	**118.6**	116.2	. . .	121.7	121.1	117.1
K^+(pyrimidine)	127.0	116.2	121.9	117.2	122.0	115.6	**117.5**	116.0	. . .	121.7	121.2	117.0
Pyrazine	122.3	122.3	115.3	122.3	122.3	115.3	. . .	121.0	116.7	. . .	121.0	116.7
H^+(pyrazine)	117.1	122.6	117.8	122.6	117.1	122.8	**118.6**	124.9	117.2	. . .	120.3	118.0
Li^+(pyrazine)	121.1	122.3	116.3	122.3	121.1	116.7	**121.6**	121.1	117.0	. . .	120.7	117.8
Na^+(pyrazine)	121.6	122.3	116.1	122.3	121.6	116.2	**121.9**	120.8	116.9	. . .	120.8	117.6
K^+(pyrazine)	122.0	122.3	115.9	122.3	122.0	115.6	**122.2**	120.6	116.9	. . .	120.9	117.5
1,3,5-Triazine	126.0	114.0	126.0	114.0	126.0	114.0	. . .	117.0	. . .	117.0	. . .	117.0
H^+(1,3,5-triazine)	121.0	116.1	125.7	116.1	121.0	120.0	**120.0**	120.8	. . .	117.1	. . .	118.2
Li^+(1,3,5-triazine)	124.9	115.0	125.3	115.0	124.9	114.7	**122.7**	117.2	. . .	117.3	. . .	117.9
Na^+(1,3,5-triazine)	125.3	114.9	125.3	114.9	125.3	114.3	**122.8**	116.9	. . .	117.3	. . .	117.8
K^+(1,3,5-triazine)	125.7	114.7	125.3	114.7	125.7	113.9	**123.1**	116.7	. . .	117.3	. . .	117.6

[a] The numbering scheme is shown in Fig. 1. X corresponds to atoms attached to the ring. When X is a hydrogen atom the bond length N–X is approximately 1, otherwise X = Li, Na, or K. Bond distances and angles involving the cation are shown in boldface.

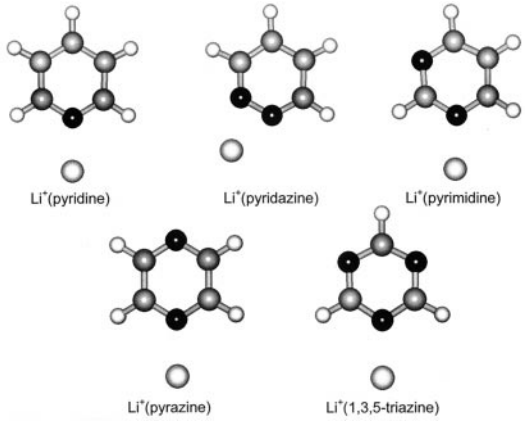

Fig. 4. Ground state geometries of Li^+(azine) complexes where azine = pyridine, pyridazine, pyrimidine, pyrazine, and 1,3,5-triazine optimized at the MP2(full)/6-31G* level of theory.

nitrogen atom produces the same protonated complex with a calculated protonation enthalpy at 0 K of 862.9 kJ/mol. The previously measured proton affinity of pyridazine, adjusted to 0 K, is 879.9 ± 16.0 kJ/mol [64,65]. As mentioned previously, this is somewhat lower than that determined for the pyridine and pyridazine systems. This also supports the conclusion that the presence of the second nitrogen atom results in a decrease in the electron density on the binding nitrogen, weakening its attraction for the proton. Because the basic sites are distant, no enhanced binding is possible in these systems. Stable cation π complexes to pyrimidine were found. These complexes were found to be 78.5, 56.1, and 33.8 kJ/mol less stable than the planar geometries for the complexes with Li^+, Na^+, and K^+, respectively. The large energy difference in the binding of the cations in the planar versus π complexes suggests that the more strongly bound planar complex should be the dominant geometry for the M^+(pyrimidine) complexes.

3.3.4. Pyrazine

Pyrazine (1,4-diazine) also possesses two basic nitrogen atoms. Protonation of pyrazine at either nitrogen atom produces the same protonated complex with a calculated protonation enthalpy at 0 K of 857.0 kJ/mol. The previously measured proton affinity of pyrazine, adjusted to 0 K, is 871.2 ± 16.0 kJ/mol [64,65]. As mentioned above, this is somewhat lower than that determined for the pyridine, pyridazine, and pyrimidine systems. Again, the presence of the second nitrogen atom results in a decrease in the electron density on the binding nitrogen, weakening its attraction for the proton. Because the basic sites are para to each other, no enhanced binding is possible in these systems.

Stable cation π complexes to pyrazine were found. These complexes were found to be 75.7, 55.7, and 33.7 kJ/mol less stable than the planar geometries for the complexes with Li^+, Na^+, and K^+, respectively. Overall, we conclude that there is only a single stable geometry for the M^+(pyrazine) complexes. The large

Table 5
Experimental and calculated enthalpies of proton and alkali metal ion binding to various azines at 0 K in kJ/mol

	Experiment		Theory
Reactant	GIBMS	Literature[a]	MP2[b]
H^+(pyridine)		924.0 (16.0)[c]	908.9
Li^+(pyridine)	181.0 (14.5)	192.5 (8.4)[d]	179.1
Na^+(pyridine)	126.7 (2.9)		123.9
K^+(pyridine)	90.3 (3.9)		91.1
H^+(pyridazine)		901.1 (16.0)[c]	894.2
Li^+(pyridazine)	234.4 (10.6)	218.4 (8.4)[d]	221.8
Na^+(pyridazine)	159.1 (3.2)		161.4
K^+(pyridazine)	130.0 (2.6)		129.6
H^+(pyrimidine)		879.9 (16.0)[c]	862.9
Li^+(pyrimidine)	154.3 (10.5)	169.6 (8.4)[d]	153.3
Na^+(pyrimidine)	102.7 (3.9)		102.7
K^+(pyrimidine)	69.4 (4.3)		72.9
H^+(pyrazine)		871.2 (16.0)[c]	857.0
Li^+(pyrazine)	149.1 (13.2)	164.5 (8.4)[d]	148.1
Na^+(pyrazine)	107.4 (3.5)		97.8
K^+(pyrazine)	67.4 (3.6)		68.5
H^+(1,3,5-triazine)		843.0 (16.0)[c]	814.4
Li^+(1,3,5-triazine)	127.4 (12.6)		125.9
Na^+(1,3,5-triazine)	88.3 (3.0)		79.8
K^+(1,3,5-triazine)	55.4 (3.0)		53.3

[a] All literature values adjusted to 0 K.
[b] Calculated at the MP2(full)/6-311+G(2*d*,2*p*) level of theory using MP2(full)/6-31G* optimized geometries with frequencies scaled by 0.9646 and including zero point energy and basis set superposition error corrections.
[c] See [64] and [65].
[d] See [25].

energy difference in the binding of the cations in the planar versus π complexes suggests that the more strongly bound planar complex should be the dominant geometry for the M^+(pyrazine) complexes.

3.3.5. 1,3,5-Triazine

1,3,5-Triazine possesses three basic nitrogen atoms. Protonation of triazine at any of the nitrogen atoms produces the same protonated complex with a calculated protonation enthalpy at 0 K of 814.4 kJ/mol. The previously measured proton affinity of 1,3,5-triazine, adjusted to 0 K, is 843.0 ± 16.0 kJ/mol. This is somewhat lower than that determined for the all of the other azine complexes. The presence of the third nitrogen atom (electron withdrawing group) results in a further decrease in the electron density on the binding nitrogen, further weakening its attraction for the proton. Because the basic sites are meta to each other, no enhanced binding is possible in these systems.

Stable cation π complexes to 1,3,5-triazine were found. These complexes were found to be 90.0, 62.3, and 36.8 kJ/mol less stable than the planar geometries for the complexes with Li^+, Na^+, and K^+, respectively. The large energy difference in the binding of the cations in the planar versus π complexes suggests that the more strongly bound planar complex should be the dominant geometry for the M^+(triazine) complexes.

3.3.6. Comparison with previous calculations

Previous calculations of the azines have all involved studies of their interactions with protons [7,26,27]. We are unaware of any studies involving the interactions of azines with the alkali metal cations. In the previous work, the proton affinities of the azines were calculated and compared to experimentally determined values. Semi-empirical methods, minimal neglect of differential overlap (MNDO) and Austin Method 1 (AM1) were unable to reproduce the correct relative basicities of these systems. Intermediate Neglect of Differential Overlap (INDO) was found to be a qualitatively better approach, but incapable of accurate energetics [27]. Ab initio calculations at levels ranging from restricted Hartree Fock (RHF) with various basis sets from STO-3G up to 6-31G* [26,27] and density functional calculations with 6-31G* and DZVP2 basis sets have also been performed [7]. All of these calculations were able to reproduce the correct relative basicities, but gave proton affinities that were consistently high. As the level of theory increased, the calculated proton affinities decreased and the agreement between theory and experiment improved. The best previous calculations performed are density functional theory calculations at the local spin density/double zeta basis set with polarization functions 2 (LSD/DZVP2) level. Values calculated at this level of theory have a mean deviation of +17.9 ± 6.3 kJ/mol from experiment. In contrast with all previous calculations, the theoretical values obtained here are lower than the measured values, with a mean deviation of −18.2 ± 9.3 kJ/mol. This relatively large deviation between theoretical and previous experimental determinations of the proton affinities of these systems is somewhat difficult to reconcile as much better agreement between theory and experiment is observed for the metalated systems examined here (discussed in the following). However, the metalated complexes are electrostatic in nature with most of the charge localized on the metal center, whereas the protonated complexes are more covalent in nature and the charge is highly delocalized. Hence, correlation effects are probably more severe, requiring the use of larger basis sets and higher levels of correlation to achieve accurate enthalpies of protonation [66].

4. Discussion

4.1. Comparison between theory and experiment

The alkali metal cation affinities of the azines at 0 K measured by guided ion beam mass spectrometry and calculated here are summarized in Table 5. The agreement between theory and experiment is very good. The mean absolute deviation between experiment and theory for the 15 alkali metal ion systems examined here is 3.3 ± 3.8 kJ/mol (and a mean deviation of 2.2 ± 4.5 kJ/mol). This is somewhat

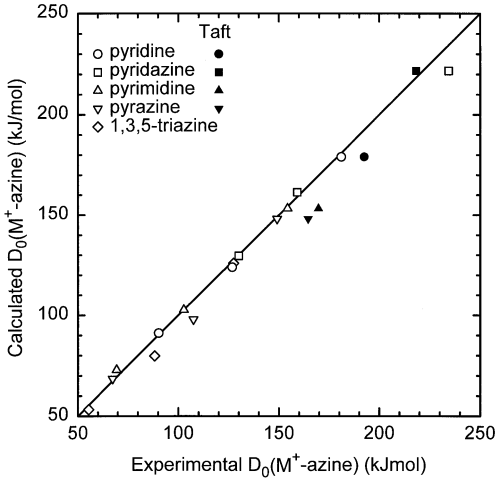

Fig. 5. Theoretical versus experimental bond dissociation energies (in kJ/mol) for M^+–azine where $M^+ = Li^+$, Na^+, and K^+ and azine = pyridine (circle), pyridazine (square), pyrimidine (triangle), pyrazine (inverted triangle), and 1,3,5-triazine (diamond). All values are at 0 K and are taken from Table 5. Experimental results include those from the present work as open signals and from Taft et al. ([25]) as closed symbols. The diagonal line indicates the values for which calculated and measured bond dissociation energies are equal.

smaller than the average experimental error of 6.4 ± 4.5 kJ/mol, and well within the expected computational accuracy (about 8 kJ/mol). The overall agreement between theory and our experimental results is shown in Fig. 5. It can be seen that the agreement is very good over the nearly 200 kJ/mol variation in binding affinities measured here. Indeed, a linear regression analysis of this comparison yields an intercept of 2.3 kJ/mol and a slope of 0.96, indicating that this level of theory reproduces the experimental results quite well.

4.2. Conversion from 0 to 298 K

To allow comparison to previous literature values and commonly used experimental conditions, we convert the 0 K bond energies determined here to 298 K bond enthalpies and free energies. The enthalpy and entropy conversions are calculated using standard formulas and the vibrational and rotational constants determined for the MP2(full)/6-31G* optimized ge-

Table 6
Enthalpies and free energies of alkali metal ion binding of M^+–azine at 298 K in kJ/mol[a]

System	ΔH_0	ΔH_0[b]	$\Delta H_{298} - \Delta H_0$[b]	ΔH_{298}	ΔH_{298}[b]	$T\Delta S_{298}$[b]	ΔG_{298}	ΔG_{298}[b]
H^+(pyridine)	924.0 (16.0)	908.9	6.0 (0.1)	930.0 (16.0)[c]	914.9	26.1 (0.1)	903.9	888.8
Li^+(pyridine)	181.0 (14.5)	179.1	2.0 (0.2)	183.0 (14.5)	181.1	27.9 (0.4)	155.1 (14.5)	153.2
Na^+(pyridine)	126.7 (2.9)	123.9	0.8 (0.2)	127.5 (2.9)	124.7	27.5 (0.5)	100.0 (2.9)	97.2
K^+(pyridine)	90.3 (3.9)	91.1	0.3 (0.1)	90.6 (3.9)	91.4	26.0 (0.6)	64.6 (3.9)	65.4
H^+(pyridazine)	901.1 (16.0)	894.2	6.1 (0.1)	907.2 (16.0)[c]	900.3	26.2 (0.1)	881.0	874.1
Li^+(pyridazine)	234.4 (10.6)	221.8	2.8 (0.2)	237.2 (10.6)	224.6	29.5 (0.3)	207.7 (10.6)	195.1
Na^+(pyridazine)	159.1 (3.2)	161.4	1.3 (0.2)	160.4 (3.2)	162.7	29.3 (0.5)	131.1 (3.2)	133.4
K^+(pyridazine)	130.0 (2.6)	129.6	0.9 (0.2)	130.9 (2.6)	130.5	28.7 (0.5)	102.2 (2.6)	101.8
H^+(pyrimidine)	879.9 (16.0)	862.9	5.9 (0.1)	885.8 (16.0)[c]	857.0	26.0 (0.1)	859.8	831
Li^+(pyrimidine)	154.3 (10.5)	153.3	2.0 (0.2)	156.3 (10.5)	155.3	28.0 (0.4)	128.3 (10.5)	127.3
Na^+(pyrimidine)	102.7 (3.9)	102.7	0.8 (0.2)	103.5 (3.9)	103.5	27.5 (0.5)	76.0 (3.9)	76.0
K^+(pyrimidine)	69.4 (4.3)	72.9	0.3 (0.1)	69.7 (4.3)	73.2	26.0 (0.6)	43.7 (4.3)	47.2
H^+(pyrazine)	871.2 (16.0)	857.0	5.9 (0.1)	877.1 (16.0)[c]	851.1	26.0 (0.1)	851.1	825.1
Li^+(pyrazine)	149.1 (13.2)	148.1	2.0 (0.2)	151.1 (13.2)	150.1	28.0 (0.4)	123.1 (13.2)	122.1
Na^+(pyrazine)	107.4 (3.5)	97.8	0.8 (0.2)	108.2 (3.5)	98.6	27.5 (0.5)	80.7 (3.5)	71.1
K^+(pyrazine)	67.4 (3.6)	68.5	0.2 (0.1)	67.6 (3.6)	68.7	26.0 (0.6)	41.6 (3.6)	42.7
H^+(1,3,5-triazine)	843.0 (16.0)	814.4	5.8 (0.1)	848.8 (16.0)[c]	808.6	25.9 (0.1)	822.9	782.7
Li^+(1,3,5-triazine)	127.4 (12.6)	125.9	2.0 (0.2)	129.4 (12.6)	127.9	28.0 (0.4)	101.4 (12.6)	99.9
Na^+(1,3,5-triazine)	88.3 (3.0)	79.8	0.7 (0.2)	89.0 (3.0)	80.5	27.5 (0.5)	61.5 (3.0)	53.0
K^+(1,3,5-triazine)	55.4 (3.0)	53.3	0.2 (0.1)	55.6 (3.0)	53.5	26.0 (0.6)	29.6 (3.0)	27.5

[a] Uncertainties are listed in parentheses.
[b] Ab initio values from calculation at the MP2(full)/6-311+G(2*d*,2*p*)//MP2(full)/6-31G* level of theory with frequencies scaled by 0.9646.
[c] See [64] and [65].

ometries, which are given in Tables 1 and 2. Table 6 lists 0 and 298 K enthalpy, free energy, and enthalpic and entropic corrections for all systems experimentally determined (from Table 3) along with the corresponding theoretical values (from Table 5). Uncertainties in the enthalpic and entropic corrections are determined by 10% variation in the molecular constants. Using these values, we have adjusted enthalpy and free energy values taken from the literature [25,64,65] (listed at 298 or 373 K) to 0 K. These are compared to the present results in Table 5 and Fig. 5.

4.3. Comparison with literature values

Table 5 and Fig. 5 also compare the present experimental results to those of Taft *et al*. [25] who used ion cyclotron resonance mass spectrometry to measure lithium ion transfer equilibria between reference species and pyridine, pyridazine, pyrimidine, and pyrazine. As can easily be seen in Fig. 5, rather poor agreement between the present results and those of Taft et al. is obtained. Their values for pyridine, pyrimidine, and pyrazine are higher than the present results by 11.5, 15.3, and 15.4 kJ/mol, respectively. However, their value for pyridazine is 16.0 kJ/mol lower than the present results and in very good agreement with theory. We have previously found that the absolute values in these studies are flawed [2]. We have suggested that the values reported in this work be adjusted downward by between 7.1 and 13.4 kJ/mol, and further that the adjustment should be toward the high end of this range. Such an adjustment of Taft's values would result in very good agreement with the present results for the pyridine, pyrimidine, and pyrazine systems, but would make agreement worse for pyridazine. Based upon this and previously found discrepancies, it seems likely that such an adjustment of Taft's values is appropriate and that the good agreement with theory without adjustment in the value of pyridazine is fortuitous.

If we consider only relative values, which Taft et al. directly measured in their experiments, their results are in qualitative agreement with ours. Namely, Li^+ binding affinities of the azines follow the order pyridazine > pyridine > pyrimidine > pyrazine. However, Taft *et al*. find that pyridazine binds 25.9 kJ/mol more strongly than pyridine to Li^+, whereas our experiments and theory suggests a much larger difference, 53.4 and 42.7 kJ/mol, respectively. The relative agreement for the other systems is much better. Taft *et al*. find that pyridine binds to Li^+ 22.9 kJ/mol more strongly than does pyrimidine. Our experiments and theory suggest similar differences between pyridine and pyrimidine of 26.7 and 25.8 kJ/mol, respectively. Taft et al. find that pyrimidine binds to Li^+ 5.1 kJ/mol more strongly than does pyrazine. Our experiments and theory both suggest a difference between pyrimidine and pyrazine of 5.2 kJ/mol. These comparisons again suggest that an adjustment of Taft's values is appropriate and that the relative value they measured for pyridazine is most likely in error. Burk and co-workers [67] have recently revised the lithium cation basicity scale originally determined by Taft and co-workers [25] based upon new experimental and theoretical results, as well as, a re-evaluation of the thermal corrections made in the Taft study. In the newly revised and expanded lithium cation affinity scale, all of Taft's values are systematically lowered by 10.9 kJ/mol in agreement with our previous conclusions [2] and resulting in very good agreement with the present results for all systems except pyridazine.

4.4. Trends in the binding of alkali metal ions to the azines

It is well established that both electrostatic and inductive interactions are the prevailing interactions responsible for the strength of binding of alkali metal ions to neutral ligands. Therefore trends in the binding energies of such metal–ligand complexes can often be understood by correlating the binding affinity with the dipole moment of the ligand. However, symmetry in the ligand can cause cancellation of local dipole interactions resulting in no overall dipole moment in the molecule, as is the case for the pyrazine and triazine systems examined here. In addition, the metal ion interacts primarily with the lone pair of electrons on only one of the N atoms in these and the pyrimidine systems. Therefore, it is unable to align itself

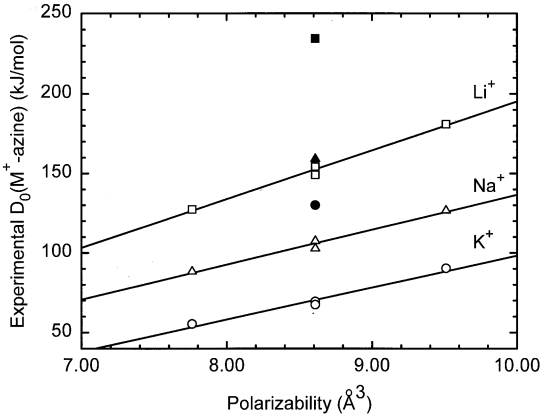

Fig. 6. Measured bond dissociation energies of M^+–azine (in kJ/mol) vs. estimated polarizability (in Å^3) of the neutral azine where $M^+ = Li^+$ (square), Na^+ (triangle), and K^+ (circle) and azine = pyridine, pyridazine, pyrimidine, pyrazine, and 1,3,5-triazine. Pyridazine values are indicated by solid symbols. Lines are linear regression fits to the data for each metal system excluding pyridazine.

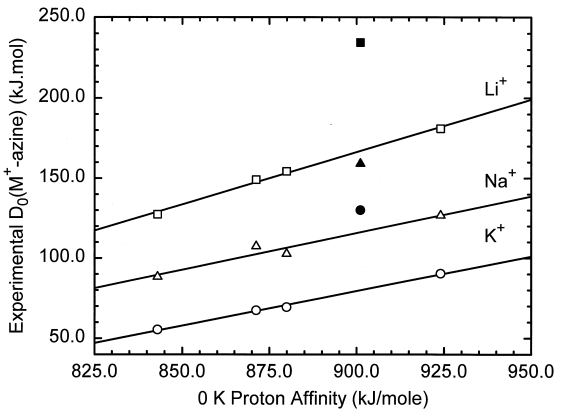

Fig. 7. Measured bond dissociation energies of M^+–azine (in kJ/mol) vs. proton affinity (in kJ/mol) of the neutral azine where $M^+ = Li^+$ (square), Na^+ (triangle), and K^+ (circle) and azine = pyridine, pyridazine, pyrimidine, pyrazine, and 1,3,5-triazine. Pyridazine values are indicated by solid symbols. Lines are linear regression fits to the data for each metal excluding pyridazine.

along the molecular dipole moment in the pyrimidine system as well. This suggests that metal ion binding to pyrimidine, pyrazine and triazine is dominated by local dipole interactions. The local dipole moments in these systems should be of comparable magnitude and can be expected to be ~2.2–2.4 D. This estimate is based upon comparison to the pyridine system and of breaking down the molecular dipole moment into two local dipole moments in the pyridazine and pyrimidine systems. Thus it is expected that the ion–dipole or ion–local dipole interactions would be very similar in the pyridine, pyrimidine, pyrazine, and triazine systems. Further, it should be significantly greater in the pyridazine systems where the metal ion is aligned with the much larger molecular dipole moment of this molecule. Indeed, this is exactly what is observed.

We can further understand the relative trends in the binding energies by correlating the binding energies with the polarizabilities of the azines and considering the binding geometry. As can be seen in Fig. 6, the correlation between the metal ion binding energies and the polarizabilities is very good for the four systems that interact through only one N atom. The larger dipole moment and the ability to interact with more than one lone pair of electrons significantly enhance the binding energy in the pyridazine system.

Similarly, we can correlate the alkali metal ion binding energies of the azines to their proton affinity. Fig. 7 shows that the correlation between the metal ion binding energies and their proton affinities is very good for four of the five azines examined here. This linear correlation suggests that the binding is very similar in the protonated and metalated complexes for these systems. However, pyridazine again deviates from this simple trend supporting the theoretical results, which find that the binding in the protonated and metalated systems is quite different. Bridging found in the metalated complexes of pyridazine is not possible with the much smaller proton and significantly enhances the binding of the metal ions relative to the proton. Alternatively, this enhancement can be thought of as resulting from the proton interacting with a smaller local dipole moment of the molecule whereas the metal ion aligns itself with the large molecular dipole moment. Comparison of the measured metal ion binding energies to that expected based upon the correlation found for the other azines shows that the percent relative enhancement is fairly similar for Li^+ and Na^+ (~39%), but is somewhat greater in the K^+ system (63%). This is relatively

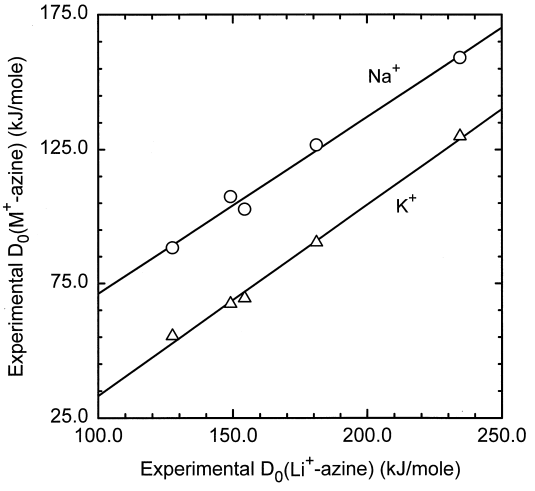

Fig. 8. Bond dissociation energies of M^+–azine (in kJ/mol) vs. bond dissociation energies of Li^+–azine (in kJ/mol) where M^+ = Na^+ (circle) and K^+ (triangle) and azine = pyridine, pyridazine, pyrimidine, pyrazine, and 1,3,5-triazine. Lines are linear regression fits to the data for each metal.

easy to understand, as it is well known that ion–dipole and ion–induced dipole interactions become more dominant as the size of the alkali metal ion increases. It is therefore not surprising that the greatest enhancement in the binding energy is observed in the K^+ systems. Based upon the same reasoning, Na^+ systems should show a larger enhancement in the binding energy than the Li^+ systems. This may suggest that our measured binding energy for Li^+–pyridazine may be slightly high, in agreement with the theoretical results. However, the approximately equal enhancement in the Li^+ and Na^+ binding energies for all of these systems suggests that the interaction is not quite so simple. And that there is a tradeoff between the enhanced binding as a result of good alignment with the molecular dipole moment and the covalent like interaction with the lone pair in these systems.

Finally, we can correlate the metal ion binding energies of Na^+ and K^+ with the azines to those determined for Li^+. Fig. 8 shows that the correlation between the Na^+ and K^+ binding energies and their Li^+ binding energies is very good for all five azines examined here. This again suggests that the binding interactions are very similar for all of the metals examined. Note, however, that this comparison shows no indication that the measured binding energy for Li^+ to pyridazine is disproportionately high compared to those for the other metal cations.

5. Conclusions

The kinetic energy dependence of the collision-induced dissociation of M^+(azine), where M^+ = Li^+, Na^+, and K^+ and azine = pyridine, pyridazine, pyrimidine, pyrazine, and 1,3,5-triazine, with Xe are examined in a guided ion beam mass spectrometer. The dominant dissociation process in all cases is loss of the intact azine ligand. Thresholds for these processes are determined after consideration of the effects of reactant internal energy, multiple collisions with Xe, and lifetime effects (using methodology described in detail elsewhere) [3]. Insight into the structures and binding of the alkali metal ions to the azines is provided by ab initio calculations of these complexes performed at the MP2(full)/6-311+G(2*d*,2*p*)//MP2(full)/6-31G* level of theory. Excellent agreement between the experimentally determined alkali metal ion affinities and *ab initio* calculations is obtained. These results suggest that these systems provide reliable anchors for the alkali metal cation affinity scales and cover a broad range of binding energies.

Acknowledgements

The authors thank P.B. Armentrout for allowing us to use the guided ion beam mass spectrometer used to conduct these experiments. This work was supported in part by an ASMS Research Award from Micromass.

References

[1] M.T. Rodgers, P.B. Armentrout, J. Phys. Chem. A 101 (1997) 1238.
[2] M.T. Rodgers, P.B. Armentrout, J. Phys. Chem. A 101 (1997) 2614.
[3] M.T. Rodgers, K.M. Ervin, P.B. Armentrout, J. Chem. Phys. 106 (1997) 4499.

[4] M.T. Rodgers, P.B. Armentrout, Int. J. Mass Spectrom. 185/186/187 (1999) 359.
[5] M.T. Rodgers, P.B. Armentrout, J. Phys. Chem. A 103 (1999) 4955.
[6] P.B. Armentrout, M.T. Rodgers, J. Phys. Chem. A, in press.
[7] P. Mátyus, K. Fugi, K. Tanaka, Tetrahedron 50 (1994) 2405.
[8] (a) A.J. Boulton, A. McKillop, in Comprehensive Heterocyclic Chemistry, A.R. Katritzky, C.W. Rees (Eds.), Pergamon, Oxford, 1984, Vol. 2, p. 7; (b) M. Tisler, B. Stanovnik, ibid, Vol. 3, pp. 2–3; (c) A.E.A. Porter, ibid., Vol. 3, pp. 158–162.
[9] K.J. Miller, J. Am. Chem. Soc. 112 (1990) 8533.
[10] R.M. Acheson, An Introduction to the Chemistry of Heterocyclic Compounds, Wiley-Interscience, New York, 1967, p. 188.
[11] F. Brody, P.R. Ruby, in Heterocyclic Compounds, Pyridine and Derivatives, E. Klingsberg (Ed.), Interscience, New York, 1960, Part 1, p. 99.
[12] R.T. Coutts, A.F. Casy, in Pyridine and Its Derivatives, R.A. Abramovitch (Ed.), Wiley, New York, 1975, Suppl. Part 4, p. 445.
[13] T.L. Gilchrist, Heterocyclic Chemistry, 3rd ed., Longman, Singapore, 1997, p. 125.
[14] M. Tísler, B. Stanovnik, in Advances in Heterocyclic Chemistry, A.R. Katritzky, A.J. Boulton (Eds.), Academic, New York, 1968, Vol. 9, p. 211.
[15] R.N. Castle, The Chemistry of Heterocyclic Compounds, Vol. 28 Pyridazines, Wiley-Interscience, New York, 1973.
[16] D.J. Brown, The Chemistry of Heterocyclic Compounds, Vol. 16 The Pyrimidines, Wiley-Interscience, New York, 1962.
[17] A.E.A. Porter, in Comprehensive Heterocyclic Chemistry, A.R. Katritzky, C.W. Rees (Eds.), Pergamon, New York, 1984, Vol. 3, p. 157.
[18] G.B. Barlin, The Chemistry of Heterocyclic Compounds Vol. 41 The Pyrazines, Wiley-Interscience, New York, 1982.
[19] V. Kaim, Angew. Chem. Int. Ed. Engl. 22 (1983) 171.
[20] J.M.E. Quirke, in Comprehensive Heterocyclic Chemistry, The Structures, Reactions, Syntheses and Uses of Heterocyclic Compounds, A.J. Boulton, A. McKillop (Eds.), Pergamon, New York, 1984, Vol. 3 Part 2B, p. 457.
[21] P.B. Farmer, in Anticancer Drugs: Reactive Metabolism and Drug Interactions, G. Powis (Ed.), Pergamon, New York, 1994, p. 1.
[22] M. D'Incalci, in Anticancer Drugs: Reactive Metabolism and Drug Interactions, G. Powis (Ed.), Pergamon, New York, 1994, p. 157.
[23] D. Bartholomew, in Comprehensive Heterocyclic Chemistry II, A Review of the Literature 1982–1995, A.J. Boulton (Ed.), Pergamon, New York, 1996, p. 575.
[24] W. Pfleiderer, in Topics in Heterocyclic Chemistry, R.N. Castle (Ed.), Wiley-Interscience, New York, 1969, p. 56ff.
[25] R.W. Taft, F. Anvia, J.-F. Gal, S. Walsh, M. Capon, M.C. Holmes, K. Hosn, G. Oloumi, R. Vasanwala, S. Yazdani, Pure Appl. Chem. 62 (1990) 17.
[26] O. Mó, J.L.G. de Paz, M. Yáñez, J. Mol. Struct. (Theochem) 150 (1987) 135.
[27] J.F. Sanz, J. Anguiano, J. Vilarrasa, J. Comput. Chem. 9 (1988) 784.
[28] K.M. Ervin, P.B. Armentrout, J. Chem. Phys. 83 (1985) 166.
[29] R.H. Schultz, P.B. Armentrout, Int. J. Mass Spectrom. Ion Processes 107 (1991) 29.
[30] E. Teloy, D. Gerlich, Chem. Phys. 4 (1974) 417; D. Gerlich, Diplomarbeit, University of Freiburg, Federal Republic of Germany, 1971; Adv. Chem. Phys. 82 (1992) 1.
[31] N.F. Dalleska, K. Honma, P.B. Armentrout, J. Am. Chem. Soc. 115 (1993) 12125.
[32] N. Aristov, P.B. Armentrout, J. Phys. Chem. 90 (1986) 5135.
[33] D.A. Hales, P.B. Armentrout, J. Cluster Sci. 1 (1990) 127.
[34] N.F. Dalleska, K. Honma, L.S. Sunderlin, P.B. Armentrout, J. Am. Chem. Soc. 116 (1994) 3519.
[35] R.H. Schultz, K.C. Crellin, P.B. Armentrout, J. Am. Chem. Soc. 113 (1992) 8590.
[36] F.A. Khan, D.C. Clemmer, R.H. Schultz, P.B. Armentrout, J. Phys. Chem. 97 (1993) 7978.
[37] R.H. Schultz, P.B. Armentrout, J. Chem. Phys. 96 (1992) 1046.
[38] E.R. Fisher, B.L. Kickel, P.B. Armentrout, J. Phys. Chem. 97 (1993) 10204.
[39] GAUSSIAN 98, Revision A.3, M.J. Frisch, G.W. Trucks, H.B. Schlegel, G.E. Scuseria, M.A. Robb, J.R. Cheeseman, V.G. Zakrzewski, J.A. Montgomery Jr., R.E. Stratmann, J.C. Burant, S. Dapprich, J.M. Millam, A.D. Daniels, K.N. Kudin, M.C. Strain, O. Farkas, J. Tomasi, V. Barone, M. Cossi, R. Cammi, B. Mennucci, C. Pomelli, C. Adamo, S. Clifford, J. Ochterski, G.A. Petersson, P.Y. Ayala, Q. Cui, K. Morokuma, D.K. Malick, A.D. Rabuck, K. Raghavachari, J.B. Foresman, J. Cioslowski, J.V. Ortiz, B.B. Stefanov, G. Liu, A. Liashenko, P. Piskorz, I. Komaromi, R. Gomperts, R.L. Martin, D.J. Fox, T. Keith, M.A. Al-Laham, C.Y. Peng, A. Nanayakkara, C. Gonzalez, M. Challacombe, P.M.W. Gill, B. Johnson, W. Chen, M.W. Wong, J.L. Andres, C. Gonzales, M. Head-Gordon, E.S. Replogle, J.A. Pople, Gaussian, Inc., Pittsburgh PA, 1998.
[40] S. Hoyau, K. Norrman, T.B. McMahon, G. Ohanessian, J. Am. Chem. Soc. 121 (1999).
[41] B.C. Guo, B.J. Conklin, A.W. Castleman, J. Am Chem. Soc. 111 (1989) 6506.
[42] J.B. Foresman, Æ. Frisch, Exploring Chemistry with Electronic Structures Methods, 2nd ed., Gaussian, Pittsburgh, 1996.
[43] S.F. Boys, R. Bernardi, Mol. Phys. 19 (1979) 553.
[44] F.B. Van Duijneveldt, J.G.C.M. van Duijneveldt-van de Rijdt, J.H. van Lenthe, Chem. Rev. 94 (1994) 1873.
[45] S.E. Hill, E.D. Glendening, D. Feller, J. Phys. Chem. A 101 (1997) 6125; S.E. Hill, D. Feller, E.D. Glendening, ibid. 102 (1998) 3813.
[46] J.B. Nicholas, B.P. Hay, D.A. Dixon, J. Phys. Chem. 103 (1999) 1394.
[47] T.S. Beyer, D.F. Swinehart, Comm. Assoc. Comput. Machines 16 (1973) 379; S.E. Stein, B.S. Rabinovitch, J. Chem. Phys. 58 (1973) 2438; Chem. Phys. Lett. 49 (1977) 1883.
[48] J.A. Pople, H.B. Schlegel, K. Raghavachari, D.J. DeFrees, J.F. Binkley, M.J. Frisch, R.F. Whitesides, R.F. Hout, W.J. Hehre, Int. J. Quant. Chem. Symp. 15 (1981) 269; D.J. DeFrees, A.D. McLean, J. Chem. Phys. 82 (1985) 333.
[49] E.V. Waage, B.S. Rabinovitch, Chem. Rev. 70 (1970) 377.

[50] W.J. Chesnavich, M.T. Bowers, J. Phys. Chem. 83 (1979) 900.
[51] P.B. Armentrout, in Advances in Gas Phase Ion Chemistry, N.G. Adams, L.M. Babcock (Eds.), JAI, Greenwich, 1992, Vol. 1, pp. 83–119.
[52] See, for example L.S. Sunderlin, P.B. Armentrout, Int. J. Mass Spectrom. Ion Processes 94 (1989) 149.
[53] M.B. More, E.D. Glendening, D. Ray, D. Feller, P.B. Armentrout, J. Phys. Chem. 100 (1996) 1605.
[54] D. Ray, D. Feller, M.B. More, E.D. Glendening, P.B. Armentrout, J. Phys. Chem. 100 (1996) 16116.
[55] F. Meyer, F.A. Khan, P.B. Armentrout, J. Am. Chem. Soc. 117 (1995) 9740.
[56] See for example, Fig. 1 in [31].
[57] P.B. Armentrout, J. Simons, J. Am. Chem. Soc. 114 (1992) 8627.
[58] F. Meyer, F.A. Khan, P.B. Armentrout, J. Am. Chem. Soc. 117 (1995) 9740.
[59] C. Lifshitz, Adv. Mass Spectrom. 11 (1989) 113.
[60] Figures were generated using the output of GAUSSIAN 98 geometry optimizations in Hyperchem™ Computational Chemistry Software Package, Version 5.0, Hypercube Inc., 1997.
[61] C. Møller, M.S. Plesset, Phys. Rev. 46 (1934) 618.
[62] R.J. Bartlett, Annu. Rev. Phys. Chem. 32 (1981) 359.
[63] W.J. Hehre, L. Radom, P.v.R. Schleyer, J.A. Pople, Ab Initio Molecular Orbital Theory, Wiley, New York, 1986.
[64] M. Meot-Ner, J. Am. Chem. Soc. 101 (1979) 2396.
[65] E.P. Hunter, S.G. Lias, Proton Affinity Evaluation in NIST Chemistry WebBook, NIST Standard Reference Database Number 69, W.G. Mallard, P.J. Lindstrom (Eds.), National Institute of Standards and Technology, Gaithersburg MD, 1998, (http://webbook.nist.gov).
[66] J.E. Del Bene, I. Shavitt, Int. J. Quantum Chem. Symp. Quantum Chem. Symp. 23 (1989) 445.
[67] P. Burk, I.A. Koppel, I. Koppel, R. Kurg, J.-F. Gal, P.-C. Maria, M. Herreros, R. Notario, J.-L.M. Abboud, F. Anvia, R.W. Taft, unpublished.